Applied Clay Science 279 (2026) 108053

Contents lists available at ScienceDirect

Applied Clay Science

journal homepage: www.elsevier.com/locate/clay

Research Paper

Adsorption of phospholipids onto layered silicate surface: The case of clinochlore

Gianfranco Ulian, Giacomo Trondoli, Francesca Ranellucci, Giovanni Valdrè *

Dipartimento di Scienze Biologiche, Geologiche e Ambientali, Università di Bologna "Alma Mater Studiorum", Plesso di Mineralogia, Piazza di Porta San Donato 1, 40126 Bologna, Italy

ARTICLE INFO

Keywords:
Clinochlore
Phospholipids
Supported lipid bilayer
Adsorption process
Density Functional Theory

ABSTRACT

The adsorption of phospholipids on clay minerals is an important research topic for both increasing the knowledge of prebiotic chemistry processes and the development of new biotechnological/pharmaceutical applications using natural components. However, atomic-scale information on the intimate relationship between lipids and clays is still missing in the scientific literature. The present work reports a detailed Density Functional Theory investigation of the adsorption of a simple phospholipid molecular model, i.e., 1, 2-divaleroyl-*sn*-glycero-3-phosphatidic acid (DVPA) and clinochlore, a phyllosilicate presenting an alternate stacking of hydrophobic brucite-like (B) and hydrophilic talc-like (TOT) layers. The results of the simulations, in absence of solvents and considering different surface coverages, showed that both substrates could condense DVPA, albeit with a general preference of the biomolecule for the B surface over the TOT one. Polar contacts were established between the DVPA and the substrates, originating mainly from the $-PO_4H_2$ group of the phospholipids. The presence of acidic (Al^{III}/Si^{IV} substitutions) and basic (Al^{III}/Mg^{II}) Brønsted-Lowry sites on the TOT and B layers, respectively, deeply increased the adsorption strength between DVPA and the substrates. The obtained results, encompassing both the molecular conformation on the clinochlore surface and the molecule/substrate binding energy, provided further knowledge on the phospholipid-mineral interactions, which could be very useful to devise innovative applications in biotechnology and environmental fields.

1. Introduction

The study of the interaction between biomolecules and inorganic substrates is a continuously unloosing interests that spans over many and different disciplines. On one side, the scientific questions towards the origin of life and prebiotic chemistry are still posing several concerns regarding the formation of complex biomolecules such as DNA/RNA and proteins from their simpler monomers, nucleotides and amino acids, respectively, whose condensation reaction (polymerisation) is a well-known thermodynamic issue in water environment (Lambert, 2008). On the other side, new nanotechnological, biochemical and biomaterials discoveries and applications may be devised from a complete understanding of the solid–liquid interfaces and their properties. For instance, characterising how proteins and nucleic acids interact and behave on the cell membranes (phospholipidic systems) is a key knowledge that may assist in drug design and delivery (Gromelski et al., 2009).

Regarding cellular membranes, which are semipermeable boundaries encapsulating cell organelles, several hypotheses and theories about their structure and functions have been proposed and developed since the beginning of the XX century, as detailedly reviewed by Bagatolli and Stock (2021). Nowadays, the consensus is that they are made of bilayers of phospholipids (mainly phosphatidylcholines, PCs) forming the so-called lipid rafts, i.e., dynamic assemblies at the nanoscale enriched in sphingolipid, cholesterol, and anchored proteins (Hancock, 2006; Lingwood and Simons, 2010). The building blocks of the membranes, phospholipids, or phosphatidic acids (PAs), are organic macromolecules made of three components; (i) glycerol (propane-1,2,3-triol $C_3H_8O_3$), (ii) two long chains of (saturated or unsaturated) fatty acids (commonly named "tails"), and (iii) a phosphate group (PO_4^{3-}, the "head" of the molecule) that can be either fully or partially protonated. Each fatty acid is bound to glycerol through an ester bond between the carboxylic group of the former and an alcoholic one of the latter, and the two acyl chains are attached to the glycerol at carbon positions C1 and C2, whereas the phosphate head is attached to C3 (see Fig. 1a). From a physical-chemical perspective, a phospholipid is then an amphiphilic molecule because the phosphate (or phosphocoline) head is polar

* Corresponding author.
E-mail address: giovanni.valdre@unibo.it (G. Valdrè).

https://doi.org/10.1016/j.clay.2025.108053
Received 29 May 2025; Received in revised form 29 October 2025; Accepted 15 November 2025
Available online 20 November 2025

(hydrophilic), whereas the two tails are apolar (hydrophobic).

In the biological and pharmaceutical research fields, the investigation of cellular membranes often involves biomembrane model systems that mimic the properties of the membrane itself. Important examples are the Langmuir monolayers (Brezesinski and Möhwald, 2005), unilamellar phospholipid vesicles and supported lipid bilayers (SLBs) (Reimhult et al., 2003), each one presenting specific and peculiar applications. A lipid monolayer at the air/liquid interface is suitable to characterise interactions with components dissolved in the water phase. Vesicles present a spherical shell formed by a bilayer of phospholipids that separate the internal ("intracellular") liquid volume from the environment ("extracellular" space). Conversely, SLBs are planar and (virtually infinite) two-dimensional systems where the phospholipids are adsorbed onto a suitable solid substrate. There are several preparation methods for synthesizing SLBs for specific applications, all derived from the pioneering work of McConnell et al. (1986) in which vesicles dispersed in a solvent are adsorbed onto a suitable surface, then they break and fuse after the surface density reaches a critical value, eventually forming a planar bilayer. It is then of utmost importance to select and employ specific substrates that are able to interact with the phospholipids in a way that preserve the physical properties of the cell membrane.

One of the key questions related to this matter concerns understanding if both specific and non-specific surface chemistry of the solid surface may affect the stability of the adsorbed, self-assembled phospholipid structures, a knowledge relevant in several applications (prebiotic and biogeochemistry, environmental studies, industrial and biomedical processes). For instance, it was suggested that the first forms of cellular life (protocells) presented a micellar-like structure where the membrane was made of single-chain fatty acids and their ester, and that the stability of these micelles in contact with minerals, e.g., silicate and oxides, may depend on the chemical and physical properties of the involved surfaces (Xu et al., 2009). Moreover, biomineralization processes carried out by different organisms (diatoms, sponges, bacteria, and humans) to synthesise minerals (amorphous silica, calcite spicules, magnetite and biological apatite, respectively) involve intimate interactions between lipid and minerals, as their precipitation occurs in a volume defined by phospholipid membranes (Ali, 1986; Boskey, 2007). In geological and industrial applications, amphiphilic molecules are also employed to prevent acid mine drainage by inhibiting the oxidation of pyrite FeS_2 (Zhang et al., 2006) and to increase the recovery of ore minerals with different techniques such as froth flotations and lubrication (Ulman, 1996; Fuerstenau, 2005), to cite some examples.

In this context, clay minerals were proven promising substrates for the deposition, condensation and catalysis of biomolecules (Heinz, 2012; Pietrement et al., 2018), as their chemical, physical and surface properties could play a significant role in mineral–environment interactions and related applications (Valdrè et al., 2011a; Moro et al., 2016). These properties at the micro- and nano-scales are relevant for controlling important interaction processes, such as adsorption, coagulation, aggregation, sedimentation, filtration, and ionic transport in porous media. In particular, by using both experimental (atomic force microscopy, AFM) and Density Functional Theory (DFT) approaches, it was demonstrated the presence of zeolitic-type Brønsted–Lowry (BL) sites in the tetrahedral-octahedral-tetrahedral (TOT) layer on atomic flat surfaces of clinochlore (Valdrè et al., 2011b). The BL sites in zeolites and clay minerals as well could also drive important adsorption and catalytic processes that can be exploited in different kinds of applications (Stueckenschneider et al., 2014). These features may be extremely valuable in the design of nano-structured hybrid materials based on natural substrates (e.g., clay minerals) that interact with bio-organic components, such as proteins and lipids. For example, it was recently shown the capability of micro-fibrous sepiolite and layered double hydroxides in assisting self-assembly of phospholipids into bilayer membranes that provide a non-degrading immobilization of viral particles and DNA (Wicklein et al., 2016) and thermal stability of the nano-hybrid compounds.

The ideal crystal structure of clinochlore [$Mg_6Si_4O_{10}(OH)_8$] was reported in Fig. 1b, where it can be noted the alternate stacking of brucite-like $Mg_3(OH)_6$ layers (labelled as O′ or B) and talc-like ones (TOT). Upon cleavage, the (001) surface of clinochlore may present remnants of B layers onto intact TOT layers, or vice versa, thus this mineral exhibits at the same time two distinct layers, with hydroxyl groups (B) and siloxane hexagonal-like rings (TOT), each one characterised by specific adsorption properties and thicknesses (about 0.4 nm and 1.0 nm for B and TOT, respectively). However, it is known that this phyllosilicate naturally presents abundant Al(III) substitutions in the B layer (Al^{III}/Mg^{II}) and in the tetrahedral sheet of the TOT layer (Al^{III}/Si^{IV}), as well as other elements that can occupy different anionic/cationic sites in different amounts. Thus, the B layer exhibits a positive charge and hydrophobic behaviour, conversely, the TOT layer is hydrophilic with a negative charge on the surface (Valdrè et al., 2009; Moro et al., 2019a).

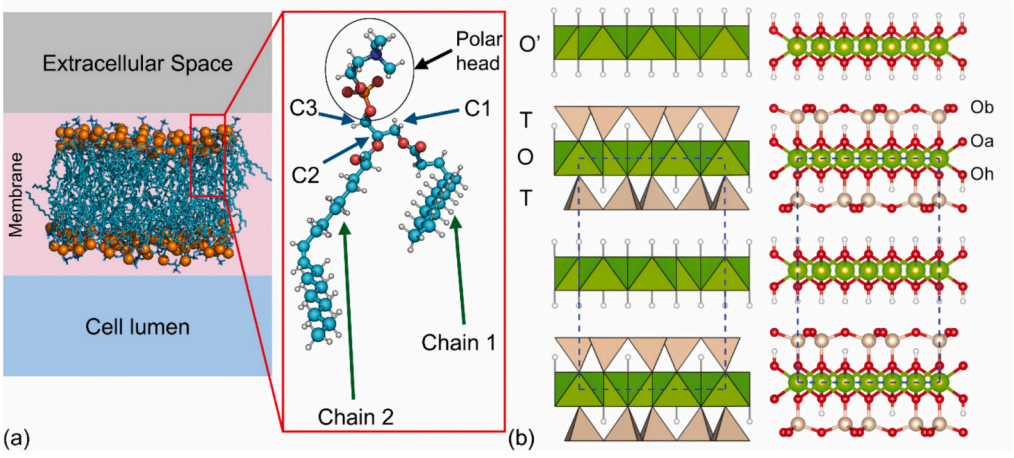

Fig. 1. (a) Schematical representation of a typical cell membrane section made of a phosphatidylcoline bilayer, highlighting the internal (lumen) and the extracellular spaces of the cell. The inset shows a ball-and-stick model of a single phospholipid molecule (1,2-dimyristoyl-*sn*-glycero-3-phosphocoline) made of two fatty acid chains bound to carbon C1 and C2 of glycerol via ester bonds and the polar head (phosphocoline) bonded to C3. (b) Polyhedral (on the left side) and ball-and-stick (on the right side) models of clinochlore, as viewed from the [100] direction. The TOT+O′ structure was highlighted in the polyhedral model, whereas the basal oxygen (Ob), apical oxygen (Oa) and hydroxyl oxygen (Oh) atoms were shown in the ball-and-stick structure. Colour coding for atoms: Si – dark yellow, Mg – green, O – red, C – cyan, H – white. The colours of the polyhedrons followed those of the central atoms (Si and Mg). (For interpretation of the references to colour in this figure legend, the reader is referred to the web version of this article.)

Differently from the ideal, stoichiometric clinochlore where the B and TOT layers are held together by dispersive forces, i.e., hydrogen bonds and van der Waals interactions, in the natural, Al-substituted mineral the bond between the layers presents a certain amount of ionic character, resulting in strong anisotropic properties (Ulian et al., 2018). Notwithstanding the electrostatic and dispersive forces acting between the stacked layers, clinochlore is easily cleavable along the [001] crystallographic direction, generally resulting in a (001) surface presenting remainders of the TOT layers above the B ones, or vice versa.

Previous AFM and DFT simulations showed how clinochlore can adsorb, organise and self-assemble both small and large biomolecules, like nucleotides (Valdrè, 2005), nucleic acids (Valdrè, 2007; Valdrè et al., 2011), amino acids (Moro et al., 2015, 2019b, 2020) and proteins (Pignataro et al., 2020), and also cells such as blood red cells (Valdrè and Fabrizioli, 2006). The results demonstrated that biomolecules are favourably and stably adsorbed onto the positively charged brucite-like layer, and only a few adsorbates were detected on the negatively charged TOT surface. Regarding simple amino acids, DFT analyses revealed that the hydrogen atom of the –COOH termination of the molecule was transferred to the oxygen atoms near the Al-substituted site.

Interestingly, the specific interaction between clay minerals and phospholipids was scarcely investigated in the scientific community. The few available works mostly characterised the formation of supported lipid bilayers on mica muscovite at the experimental and theoretical levels. For example, Jurak (2014) experimentally determined the surface Gibbs energy interaction of different phospholipids and cholesterol on muscovite, using three probe liquids (water, formamide and diiodomethane), by contact angle measurements. The author found different interaction strengths between the tested phospholipids and solvents, however, no information was reported on the bilayer/solvent interaction with the mineral substrate. Pertsin and Grunze (2014) performed molecular mechanics simulations within the grand canonical Monte Carlo approach with a SLB model made of 1,2-dilauroyl-phosphatidyl-ethanolamine (DLPE) bilayer supported on a single layer of muscovite, showing that the model membrane adhered to the substrate because of individual lipid molecules protruding from the bilayer and forming widely spaced links with the support.

However, to the authors' knowledge, there is no experimental or theoretical study focused on the interaction between phospholipids and clinochlore and, considering the peculiar features of this mineral previously described, the objective of the present work is to fill this important gap. By using very accurate, atomic-scale Density Functional Theory simulations, the adsorption of a selected model phospholipid, i.e., 1, 2-divaleroyl-*sn*-glycero-3-phosphatidic acid (DVPA), on both the brucite-like and talc-like layers of clinochlore was investigated in detail. DVPA can be considered one of the simplest phosphatidic acids, with aliphatic chains of five carbon atoms, representing a suitable starting model for this type of amphiphilic molecules. Several adsorbate/adsorbent models were realised encompassing different surface coverages to simulate the behaviour of a single molecule and of a monolayer of the phosphatidic acid. The goal was to provide the conformation of the molecules on the different clinochlore surfaces, the information about possible polar contacts between DVPA and the substrate and the strength of the lipid-mineral interaction.

2. Materials and methods

The Density Functional Theory (DFT) simulations of the present work were performed with the CRYSTAL23 code (Erba et al., 2023), which implements the Kohn-Sham equations and the self-consistent field (SCF) method.

The (001) surfaces of the building units of clinochlore, i.e., the brucite-like layer (B) and the talc-like one (TOT) were modelled by cleaving the bulk of the mineral perpendicularly to the [001] direction, realising slab models as described in Moro et al. (2015, 2016, 2019a, 2019b). The clinochlore bulk model was studied and described in previous works of some of the authors (Ulian et al., 2018, 2020).

The crystalline orbitals of the B and TOT slab models (two-dimensional systems) and the molecular ones of the 1, 2-divaleroyl-*sn*-glycero-3-phosphatidic acid (DVPA) were constructed within the linear combination of atomic orbitals (LCAO) approach, where the orbitals of each atomic species were described in terms of Gaussian-type functions (GTFs). In this work, the electronic shells of phosphorous, silicon, aluminium, magnesium, carbon, oxygen, and hydrogen were modelled using 85-21d1G (Zicovich-Wilson et al., 2002), 88-31G* (Nada et al., 1996), 85-11G* (Catti et al., 1993), 8-511d1G (Valenzano et al., 2007), 6-311d11G (Valenzano et al., 2007), 8-411d11G (Valenzano et al., 2006) and 3-1p1G (Gatti et al., 1994) basis sets, respectively. This set of GTFs was already employed to investigate the bulk and surface properties of phyllosilicates and hydroxides (Ulian and Valdrè, 2015, 2019, 2023), and to model the interactions between the cited minerals with organic molecules (Moro et al., 2019b, 2020; Ulian et al., 2021a, 2021b).

B3LYP (Lee et al., 1988; Becke, 1993a, 1993b) was chosen as DFT functional to run all the simulations because of its well-known accuracy for solid and molecular systems (Pascale et al., 2005; De La Pierre et al., 2011; Prencipe et al., 2011). This functional includes 20 % of the exact Hartree-Fock exchange and a small non-local contribution to the exchange and correlation energy. The a posteriori DFT-D3 correction was applied to include van der Waals interactions in the physical treatment of the slab models, the DVPA molecule and the adsorbate-adsorbent system. Details on the formulation and implementation of the DFT-D3 scheme were reported in dedicated literature (Grimme et al., 2010, 2011, 2015).

The total energy was calculated on a pruned grid with 75 radial points and a maximum number of 974 angular points in regions relevant to chemical bonding, subdivided into five shells with different angular grids (Erba et al., 2023). The SCF iterative calculation was considered converged when the energy difference between two consecutive steps was lower than 10^{-8} Ha. The tolerances that controlled the numerical accuracy of the Coulomb and overlap integrals were set to 10^{-8} (ITOL1 to ITOL4 keywords in CRYSTAL23), whereas ITOL5 was set to 10^{-16}. The Hamiltonian matrix was diagonalized on a Monkhorst and Pack (1976) 6×6 grid for the brucite-like slabs and 4×4 for the talc-like layer. These nets were slightly reduced for large (001) surface models to optimize the computational resources, still, a sufficient number of reciprocal space points was considered to obtain accurate results.

The unit cell parameters and atomic coordinates were relaxed at 0 K and 0 GPa using the analytical gradient method for the atomic positions and a numerical gradient for the slab cell parameters. The BFGS algorithm was adopted as the optimization method to minimize the forces between the atoms and stress acting on the 2D cell (Broyden, 1970a, 1970b; Fletcher, 1970; Goldfarb, 1970; Shanno, 1970). The tolerances for the maximum allowed gradient and the maximum atomic displacement have been set to 10^{-5} Ha bohr^{-1} and 4×10^{-5} bohr, respectively.

When surface adsorption phenomena involving periodic structures are modelled with quantum chemical methods, the binding energy *BE* per unit cell per adsorbate molecule is calculated from the following formula:

$$BE = E(\mathrm{SM//SM}) - E(\mathrm{S//S}) - E_{\mathrm{M}}(\mathrm{M//M}) \quad (1)$$

where E(SM//SM) is the energy of a fully relaxed unit cell with the molecule(s) M interacting with the slab S, E(S//S) is the energy of a fully relaxed slab, and E_{M}(M//M) is the molecular energy of the free, optimized molecule. In Eq.(1), the symbols S, M or SM before the double slash (//) indicate the system under consideration, and the symbols after the double slash specify the geometry in which the energy was calculated. According to the above formulation, the adsorbate is bound to the surface when *BE* is negative, indicating energy released after the adsorbate-adsorbent (physical or chemical) interaction. It is possible to re-write Eq.(1) to consider the energy required to change the geometry

(conformation) of both molecule and slab after the interaction, using the following formulas:

$$BE = BE^{*} + \delta E_S + \delta E_M \quad (2)$$

$$\delta E_S = E(S//SM) - E(S//S) \quad (3)$$

$$\delta E_M = E(M//SM) - E_M(M//M) = \Delta E_M + \Delta E_L \quad (4)$$

$$BE^{*} = E(SM//SM) - E(S//SM) - E(M//SM) \quad (5)$$

where δE_S represents the deformation energy of the slab surface ($\delta E_S > 0$), δE_M is the sum of the deformation energy of the molecule (ΔE_M) and the intermolecular interactions (ΔE_L) occurring between the infinite 2D replicas of the phospholipid in the slab-to-molecule (SM) configuration. The purely molecular deformation energy was computed as:

$$\Delta E_M = E_M(M//SM) - E_M(M//M) \quad (6)$$

where $E_M(M//SM)$ is the molecular (non-periodic) energy of the phospholipid with the geometry occurring on the slab surface, hence it follows that $\Delta E_M > 0$. The lateral intermolecular interactions, ΔE_L, were calculated as:

$$\Delta E_L = E(M//SM) - E_M(M//SM) \quad (7)$$

where the ΔE_L values can be either positive (indicating repulsion between the molecular replicas) or negative (attraction). According to Eq.(5), the BE^* binding energy is then free from deformational and lateral interaction contributions, because it is the result of energy differences between periodic calculations carried out at the geometry of the SM system.

Because Gaussian-type orbitals basis sets are not complete, the above BE definition msust include the basis set superposition error (BSSE) correction, using the same counterpoise method adopted for intermolecular complexes (Boys and Bernardi, 1970). The definition of the BSSE-corrected interaction energy BE^C is defined as:

$$BE^C = BE^{*C} + \delta E_S + \delta E_M \quad (8)$$

where:

$$BE^{*C} = E(SM//SM) - E(S[M]//SM) - E([S]M//SM) \quad (9)$$

$$BE^C = BE + \mathrm{BSSE} \quad (10)$$

$$\mathrm{BSSE} = BE^{*C} - BE^{*} \quad (11)$$

$E(S[M]//SM)$ and $E([S]M//SM)$ are the energy of the slab plus the ghost functions of the molecule and the energy of the infinite replica of the molecules with the ghost functions of the underneath slab, respectively. Since the variational theorem ensures that $BE^{*C} > BE^{*}$, it immediately follows that BSSE is a positive value.

All previous considerations are adequate to quantitatively describe the adsorption process occurring in a low coverage setting, i.e., when the molecule is well separated from its 2D replicas. However, if the number of molecules per surface area increases, the BE^C value could be strongly biased by lateral interactions between the phospholipids. Hence, a more appropriate way to quantify the binding energy between the phospholipid and the clinochlore layers at high coverage is the following:

$$BE_L{}^C = BE^C - \Delta E_L \quad (12)$$

where the contribution from the lateral interactions is removed from the binding energy.

3. Results

3.1. Brucite-like, talc-like and phospholipid models

As explained in the introduction, clinochlore is made of two types of layers stacked alternately along the [001] crystallographic direction. Since the brucite-like and talc-like layers are held together by dispersive forces, i.e., a mix of hydrogen bonds and van der Waals interactions, cutting the (001) surface does not break any covalent (strong) bond, and the surface reconstruction is hence small. Also, the B and TOT layers have minimal influence on each other properties, thus it is possible to consider them one at a time for the investigation of adsorption phenomena involving molecules, as already reported in previous works (Moro et al., 2015, 2016, 2020).

The B layer belongs to the trigonal crystal system with two possible space groups, i.e., $P\bar{3}m1$ and $P\bar{3}$ if the hydrogen groups are all aligned along the [001] direction or if proton disorder is allowed, respectively (Ulian and Valdrè, 2019). A geometrically optimized (001) single-layer model of B layer with space group $P\bar{3}$ ($Mg_3(OH)_6$, 15 atoms, $Z = 3$) is shown in Fig. 2a. The lattice parameters of this model were $a = b = 5.4038$ Å and $\gamma = 120°$. The calculated electrostatic surface potential (ESP), also reported in Fig. 2a, highlighted a triangular pattern of positive (on H) and negative potential (between the Mg_3O_3 hexagonal-like rings) on both sides of the slab. This two-dimensional structure was also suitable to model the Al(III)/Mg(II) vicariance observed in natural clinochlore specimens (Valdrè et al., 2009; Valdrè et al., 2011b; Moro et al., 2016), and also similar to 2:1 Mg/Al layered double hydroxides (LDH). An Al-bearing (001) B surface with a chemical formula $Mg_2Al(OH)_5O$ was reported in Fig. 2b, where the aluminium substitution was followed by the removal of a hydrogen atom from one side of the model to maintain the charge neutrality. The symmetry of this substrate lowered to $P1$ because of the substitution, and the lattice parameters of the relaxed structure were $a = 5.2686$ Å, $b = 5.2687$ Å and $\gamma = 119.86°$. As noticed from the 3D electrostatic potential, the top side of the Al-bearing B surface, where the H atom was removed, showed a strong negative potential on top of the O atom. Conversely, the bottom side presented a generally positive electrostatic potential.

Talc $Mg_3Si_4O_{10}(OH)_2$ crystallizes in the triclinic system, $P\bar{1}$ space group, with two unit formula ($Z = 2$, 42 atoms) in the unit cell (Perdikatsis and Burzlaff, 1981). Then, a single, stoichiometric (001) TOT layer of chlinochlore belongs to the $P\bar{1}$ layer group, and after geometry optimization the two-dimensional lattice parameters were $a = 5.2684$ Å, $b = 9.1251$ Å and $\gamma = 90.00°$. The ESP of this model is shown in Fig. 2c, where a pseudo-hexagonal pattern of positive potential (on the Si atoms and the H atoms of the hydroxyl groups) and negative potential (on top of the bridging oxygen of the T sheet) can be noted. To model the typical Al(III) substitutions occurring in clinochlore, two Si (IV) atoms were substituted, one per T sheet, also maintaining the $P\bar{1}$ space group. In this case, the excess of negative charge due to the Al(III)/Si(IV) vicariance was balanced by adding two hydrogen atoms near the aluminium ones on the top and bottom sides of the TOT layer, leading to a model with chemical formula $HMg_3Si_3AlO_{10}(OH)_2$. After relaxation, the unit cell parameters of the Al-substituted talc-like layer were $a = 9.2627$ Å, $b = 5.2876$ Å and $\gamma = 89.54°$. According to previous Atomic Force Microscopy (AFM) and Kelvin Probe Force Microscopy (KPFM) measurements, and quantum mechanical simulations (Valdrè et al., 2011b), this modelling approach leads to the creation of zeolitic-type Brønsted-Lowry sites on a two-dimensional surface. This can be observed from the calculated ESP of the aluminium-bearing TOT layer (Fig. 2d), where a very strong positive potential occurs on the Al-substituted site.

The model of DVPA geometrically optimized in the gas phase is reported in Fig. 2e, alongside the calculated electrostatic molecular potential (EMP). As stated in the Introduction, this is the simplest phospholipid that is made of two aliphatic chains of valeric acid (five atoms) connected to glycerol by ester bonds, and the polar head is a protonated phosphate group ($–PO_4H_2$). The carbonyl oxygen atoms of the apolar tails and the –P = O oxygen atom of the phosphate head exhibited strong negative potential. In contrast, a strong positive potential was noticed on one of the H atoms of the $–PO_4H_2$ group. The

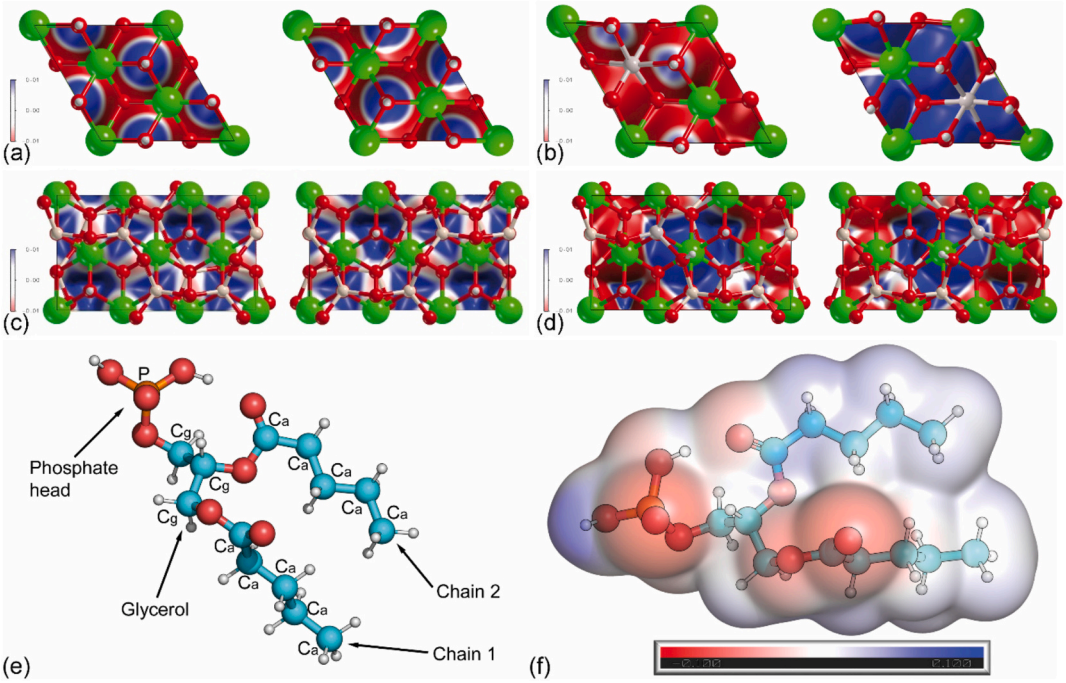

Fig. 2. Electrostatic surface potential (ESP) of (a) stoichiometric $Mg(OH)_2$ brucite, (b) Al-bearing brucite, (c) stoichiometric talc-like layer and (d) Al-substituted TOT layer. The ESP was calculated on an isosurface of 10^{-3} a.u. of charge density, with the potential ranging between ±0.01 Ha. In panels (a-d), the picture on the left refers to the top (001) surface, while the picture on the right refers to the bottom surface. (e) Stick-and-ball model of the DVPA molecule, highlighting the different structural units, and the types of carbon atoms (C_g and C_a, glycerol and aliphatic carbons, respectively.) In panel (f), the electrostatic molecular potential of DVPA was represented on an isosurface of charge density of 10^{-3} a.u. within ±0.01 Ha. Colour coding for atoms: P – orange, Si – dark yellow, Al – grey, Mg – green, O – red, C – cyan, H – white. (For interpretation of the references to colour in this figure legend, the reader is referred to the web version of this article.)

other hydrogen atom of the polar head formed an intramolecular hydrogen bond (1.82 Å) with the carbonyl O of one of the fatty acid chains. As a result, the positive potential of the H atom and the negative one of the involved O atoms were smaller in absolute value. Conversely, the apolar chains exhibited a generally small positive potential on the hydrogen atoms of the $–CH_2–$ and $–CH_3$.

The analysis of the electrostatic potential of the clinochlore surface models and the phospholipid also provided important insights into the possible adsorption sites because, according to the principle of complementarity, positive regions in the molecule would preferentially interact with negative ones on the substrate and vice versa.

3.2. Low-coverage adsorption of DVPA on the brucite-like layer

The first step in the present study was the simulation of the interaction between a single DVPA molecule and the (001) brucite-like surface, which provided a suitable adsorption substrate for several biomolecules and cells (Valdrè, 2005; Antognozzi et al., 2006; Moro et al., 2019b; Pignataro et al., 2020). This means modelling a mineral slab with a large surface area to avoid lateral interactions between the molecule in the simulation cell and those in the neighbouring cells (2D replicas).

To this aim, the following starting models of adsorption of DVPA onto the 4 × 4 stoichiometric (001) brucite surface were created:

- BP01, where DVPA was oriented horizontally to the slab;
- BP02, with DVPA oriented perpendicularly to the slab with the phosphate head pointing towards the surface;
- BP03, where DVPA was placed perpendicularly to the (001) surface and with the $–PO_4$ group pointing outwards the slab.

The naming convention adopted indicates in the first character (B) the brucite-like layer and in the second one (P) the phospholipid molecule. These models showed a coverage of 0.2 molecules nm^{-2}, which is suitable to investigate the behaviour of a single phospholipid molecule onto the brucite-like substrate. The DVPA molecule was placed at about 4 Å from the topmost atom of the (001) surface to avoid any bias in the structural relaxation of the phospholipid. However, the chosen distance allowed the establishment of molecule-to-substrate interactions, an approach that was adopted for each subsequent model that will be described and discussed.

Fig. 3 shows the relaxation results of the BP01 model, where DVPA kept a parallel orientation to the B slab. In general, DVPA did not exhibited any significant structural change beside the $C_a–C_a–O–C_g$ torsional angle variation (about −5 %) related to the second chain of the molecule and the slight reduction of the intra-chain $C_a—C_a— C_a—C_a$ dihedral angles (ca. –2.0 %), with the subscripts “a” and “g” indicating the acyl and glycerol carbon atoms, respectively. Several polar interactions, i.e., hydrogen bonds, were established between the oxygen atoms of the $–PO_4$ head of molecule and the hydrogen atoms belonging to the mineral surface. These long-range bonds occurred at 2.128 Å and 2.194 Å for the P–O–H and P–O–C oxygen atoms of the DVPA molecule, respectively. Other polar contacts at longer distances were observed for the carbonyl oxygen (C = O) of the first fatty acid chain (2.394 Å) and the second OH group linked to the phosphate head (2.413 Å). Conversely, no long-range contact was established between the valeric acid chains and the brucite surface. The (001) brucite-like surface suffered very small structural variations, mainly in the form of canting and rotation of the OH groups towards the phospholipid. These observations were in line with the calculated projected density of states (PDOS) and Crystal Orbital Overlap Population (COOP), reported in **Fig.S1a** in the Supplemental Materials. The analysis revealed several overlaps between the orbitals of the molecule and the substrate, with bonding states mainly associated with the $–PO_4$ group and H and O atoms of the substrate.

Energy data about the adsorption process of the BP01 configuration

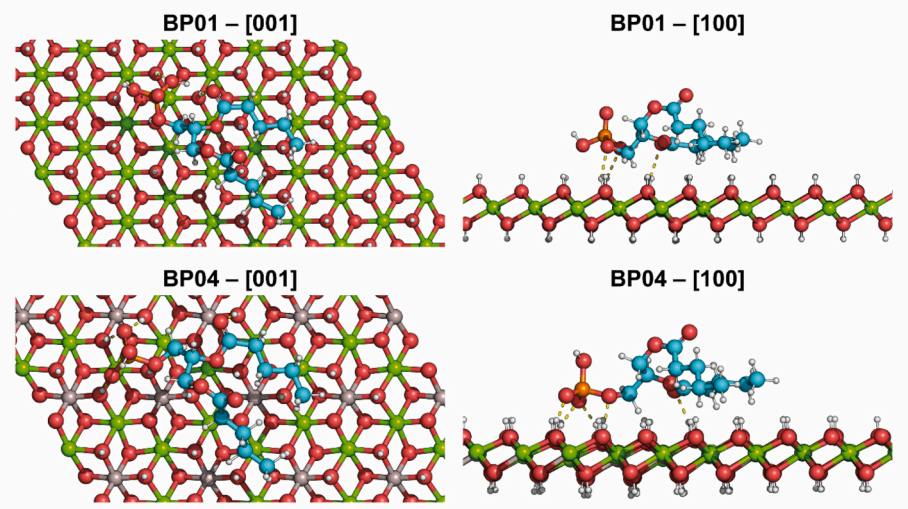

Fig. 3. Views along the [001] and [100] directions of the optimized BP01 (stoichiometric brucite-like layer) and BP04 (Al-bearing B substrate) models. Hydrogen bonds (polar contacts) between the phospholipid and the (001) mineral surface are shown in yellow dashed lines. Colour coding for atoms: P – orange, Al – grey, Mg – green, O – red, C – cyan, H – white. (For interpretation of the references to colour in this figure legend, the reader is referred to the web version of this article.)

were reported in Table 1, with a BSSE-corrected binding energy BE^C = −139.96 kJ mol^{-1}, highlighting a strong molecule-to-surface adsorption. It is interesting noting that this value is mostly a result of long-range interactions, and when the dispersive forces contribution was removed the binding energy resulted positive (about +57 kJ mol^{-1}), meaning repulsion between DVPA and the B layer. The small relaxation of both molecule and substrate were reflected in the values of ΔE_M (+5.67 kJ mol^{-1}) and δE_S (+18.15 kJ mol^{-1}), respectively. Furthermore, the very small lateral interaction (ΔE_L = +0.36 kJ mol^{-1}) suggested that the BP01 model was able to describe the interaction between a single phospholipid and the mineral surface.

The relaxation results for the BP02 and BP03 systems were graphically reported in **Fig.S2** in the Supplemental Materials. The picture showed that the DVPA molecule, initially placed perpendicular to the B substrate, rotated during the geometry optimization procedure to a planar configuration similar to that observed for the BP01 model. These results suggested that this is the preferential conformation of DVPA on this substrate, as it maximizes the interactions between the molecule and the mineral slab, particularly those related to the valeric acid chains even if no polar contact between them and the substrate were observed in the three systems (BP01–03). From the energetic perspective, the adsorption behaviour of BP02 is close to that of BP01, while more profound variations were observed in the BP03 model. Indeed, as shown in **Figs.S1c,d**, the phosphate head yielded to the mineral surface one of the hydrogen atoms of the P–OH acid groups to a hydroxyl group of the surface, creating a "water-like" molecule bound to the mineral slab. This explained the high deformation energies of the slab (δE_S = +133.20 kJ mol^{-1}) and of the molecule (ΔE_M = +674.93 kJ mol^{-1}), and the strong binding energy (BE^C = −237.94 kJ mol^{-1}) that is almost 1.5 times the one calculated for the BP01 and BP02 models. Moreover, the formation of a positive charge on the surface and a negative one on the molecule due to the H atom exchange increased the Coulomb interactions between the two systems, justifying the negative BE^C value of the BP03 model when the energy contribution from the long-range interactions was removed (see Table 1). In addition, the variations of the geometry of DVPA after adsorption onto the brucite-like slab were similar to those observed for the BP01 system.

Considering the results of the stoichiometric B substrate, the adsorption of DVPA onto the Al-bearing (001) B layer was modelled considering only the horizontal starting configuration (molecule parallel to the slab), which was labelled as BP04. The relaxed adsorbate/adsorbent system was reported in Fig. 3, where some important differences from the adsorption on the stoichiometric brucite-like slab can be noted. The first one is the proton transfer from the phosphatidic acid head group towards the oxygen atom near the Al substitution. The second difference is the establishment of many polar contacts (O — H bonds) between the phospholipid and the substrate, namely: (i) four from the –PO_4 group (between 1.777 Å and 1.828 Å), (ii) one from the carbonyl oxygen atom of the second fatty acid chain (2.013 Å) and, interestingly, (iii) a C_g – H — O interaction (1.971 Å). Also, the relaxation of the molecule on the mineral surface led to a reduction of the C_a–C_a–O–C_g torsional angle value of the second fatty acid chain of about

Table 1
Binding energies *BE* (uncorrected for the basis set superposition error, BSSE), *BE** (binding energy without contributions from substrate deformation energy δE_S, molecular deformation ΔE_M, and lateral molecular interactions ΔE_L), BE^{*C} and BE^C (*BE* and *BE** corrected for BSSE) associated with the low-coverage adsorption of DVPA onto the brucite-like layer of clinochlore. The energy values are in kJ mol^{-1}.

System	*BE*	*BE**	δE_S	δE_M	ΔE_M	ΔE_L	BE^{*C}	BE^C	*BSSE*
	Electronic + DFT-D3 energy								
BP01	−182.45	−206.62	18.15	6.02	5.67	0.36	−164.14	−139.96	42.48
BP02	−181.35	−239.95	37.98	20.61	20.97	−0.35	−194.76	−136.16	45.19
BP03	−293.26	−1101.00	133.20	674.54	674.93	−0.38	−1045.68	−237.94	55.32
BP04	−423.07	−951.38	73.70	454.60	454.21	0.39	−898.81	−370.51	52.57
	Electronic energy								
BP01	14.40	−12.08	22.33	4.15	3.72	0.43	30.40	56.88	42.48
BP02	18.51	−42.53	42.58	18.47	18.75	−0.28	2.66	63.70	45.19
BP03	−80.93	−890.08	137.30	671.85	672.16	−0.31	−834.75	−25.61	55.32
BP04	−183.83	−710.85	79.18	447.84	447.35	0.49	−658.28	−131.26	52.57

Note: $\delta E_M = \Delta E_M + \Delta E_L$.

−8.06 %. However, as for the BP01–03 models, no significant variations in the C – C, C – H and C – O bond lengths were observed.

The adsorption of DVPA on the Al-bearing B slab was highly favourable (BE^C = −370.51 kJ mol^{-1}), with a considerable electronic contribution (electronic BE^C = −131.26 kJ mol^{-1}). As noted in the BP03 model, the proton transfer led to high deformation energies for both the molecule (ΔE_M = +454.21 kJ mol^{-1}) and the mineral surface (δE_S = +73.70 kJ mol^{-1}). The PDOS/COOP analysis (**Fig.S2b**) showed an increase in the overlaps between the orbitals of the molecule and the substrate (mainly oxygen and hydrogen) compared to the BP01 system, with a mix of bonding and antibonding states involving the aliphatic chains and the oxygen and hydrogen atoms of the substrates.

3.3. Low-coverage adsorption of DVPA on the talc-like layer

Two starting models for the adsorption of the phospholipid onto the TOT layer were created. The first one, labelled TP01, used a 3 × 2 supercell of the stoichiometric (001) surface of talc (total number of atoms equal to 252); the second model was created from a supercell of the same size as the TP01 system, containing 264 atoms. The surface area of the realised slabs allowed modelling a surface coverage as low as 0.3 molecules nm^{-2}. The phosphatidic acid was placed parallel to the slab in both the TP01 and TP02 models, expecting a relaxation behaviour similar to that observed for the BP01–03 models.

A graphical representation of the geometrically optimized DVPA/TOT systems was reported in Fig. 4, whereas the energy associated with the adsorption process can be found in Table 2.

In general, as observed for models BP01–04, the lateral interaction between the molecule in the simulation cell and the replicas in neighbouring cells is very small, below the experimental uncertainties (ΔE_L between 0.20 kJ mol^{-1} and 0.89 kJ mol^{-1}). This suggested that the supercell models for the (001) TOT slabs were large enough to simulate the interaction between a single molecule and the substrate.

In both TP01 and TP02 models, the phospholipid molecule maintained the planar configuration, interacting with the substrate at a distance of about 1.88 Å and 1.92 Å, respectively, from the topmost oxygen atoms of the talc-like layer. When DVPA was adsorbed onto the stoichiometric TOT layer, no polar contact was established between the molecule and the (001) mineral surface. Minimal changes in the conformation of the phosphatidic acid were observed, with absolute variations of the C – C, C – H, C – O and P – O bond lengths and C_a – C_a – C_a – C_a (intra-fatty acid chain) dihedral angle in the range 0.04–0.36 %. Only the C_a – C_a – O – C_g dihedral angle of the second chain of the fatty acid was modified by about −3.61 %. Overall, in the TP01 system, the DVPA was adsorbed with a binding energy BE^C = −139.50 kJ mol^{-1}, meaning a strong molecule-to-substrate interaction that was very close to that obtained from the BP01 and BP02 models involving the stoichiometric brucite-like layer. Also, the contribution of the dispersive forces is of utmost importance, as the sole electronic binding energy was positive (repulsion). The small changes in the geometry of both the phosphatidic acid and mineral surface explained the very small deformation energy of the two systems, +3.68 kJ mol^{-1} and + 3.57 kJ mol^{-1}, respectively.

A slightly different adsorption behaviour was noted when the DVPA molecule interacted with the Al-defective TOT layer (model TP02). A single polar contact (1.763 Å) was established between the oxygen of one of the OH bound to the PO_4 group of the phosphatidic acid and the Brønsted-Lowry acidic site of the surface. This led to a slightly higher energy of deformation of both DVPA (ΔE_M = +15.24 kJ mol^{-1}) and substrate (δE_S = +13.92 kJ mol^{-1}), and to an increased adsorption energy compared to the stoichiometric TOT slab (BE^C = −163.15 kJ mol^{-1}). However, the pure electronic energy associated with the BE^C value was positive albeit much lower than that calculated for the TP01 model, meaning that the interaction was still driven by weak interactions. By analyzing the PDOS and COOP (see **Fig.S3**), it can be noted a that the hybridisation of the orbitals of DVPA and the TOT layers resulted in a mix of bonding and antibonding states involving the aliphatic chains and the phosphate groups, with a generally more positive COOP for the DVPA/TP02 model than the DVPA/TP01 one.

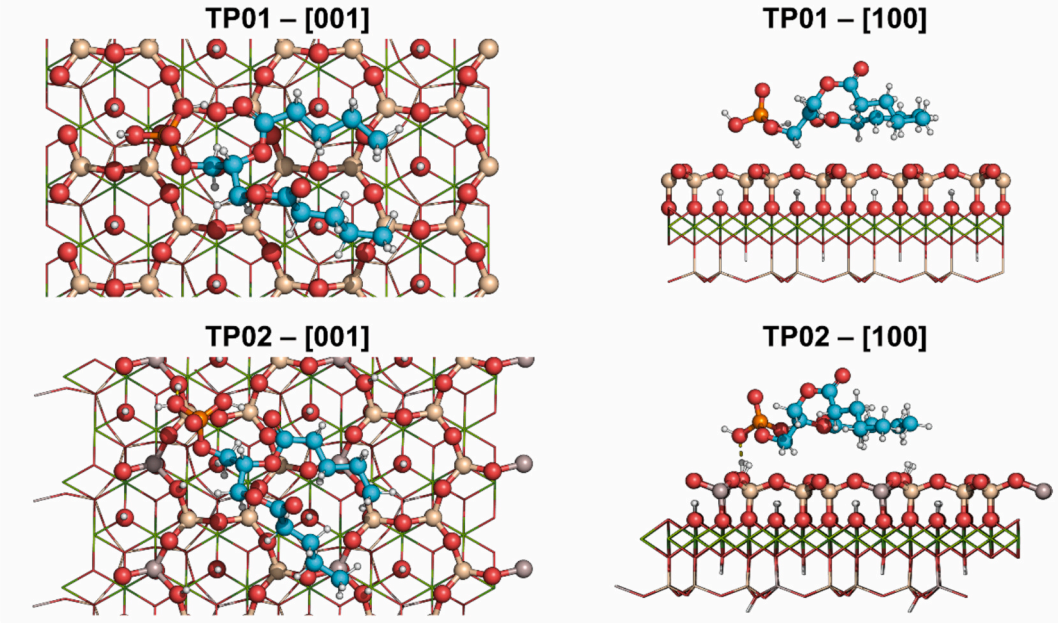

Fig. 4. Views along the [001] and [100] directions of the optimized TP01 (stoichiometric talc-like layer) and TP02 (Al-bearing TOT substrate) models. Hydrogen bonds (polar contacts) between the phospholipid and the (001) mineral surface are shown in yellow dashed lines. For the sake of clearness, only the tetrahedral sheet exposed to the surface was represented as balls-and-sticks, conversely, the other parts of the TOT layer were shown as coloured wireframes. Colour coding for atoms: P – orange, Si – dark yellow, Al – grey, Mg – green, O – red, C – cyan, H – white. (For interpretation of the references to colour in this figure legend, the reader is referred to the web version of this article.)

Table 2
Binding energies *BE* (uncorrected for the basis set superposition error, BSSE), *BE** (binding energy without contributions from substrate deformation energy δE_S, molecular deformation ΔE_M, and lateral molecular interactions ΔE_L), BE^{*C} and BE^C (*BE* and *BE** corrected for BSSE) associated with the low-coverage adsorption of DVPA onto the TOT layer of clinochlore. The energy values are in kJ mol^{-1}.

System	*BE*	*BE**	δE_S	δE_M	ΔE_M	ΔE_L	BE^{*C}	BE^C	*BSSE*
	Electronic + DFT-D3 energy								
TP01	−157.68	−165.50	3.57	4.24	3.68	0.56	−139.50	−131.69	25.99
TP02	−192.41	−221.76	13.92	15.44	15.24	0.20	−192.51	−163.15	29.25
	Electronic energy								
TP01	36.65	27.88	5.61	3.16	2.27	0.89	53.87	62.65	25.99
TP02	−2.29	−32.69	17.11	13.29	12.79	0.50	−3.44	26.96	29.25

Note: $\delta E_M = \Delta E_M + \Delta E_L$.

3.4. Increased coverage of phospholipid on the brucite-like layer

To simulate the formation of a phospholipid monolayer on the (001) brucite substrate, the lateral dimensions of the brucite-like slab models were reduced, and the surface coverage increase was modelled by placing the DVPA molecules vertically with respect to the (001) plane. In these conditions, lateral interactions were expected being more relevant in the monolayer formation and in the molecule-to-substrate interactions.

Several models were developed, briefly depicted in the following:

- BP05 and BP06, with a 3 × 2 stoichiometric (001) brucite-like slab (initial s.g. $P\bar{3}m1$), placing the phospholipid with the –PO_4 group pointing outwards and towards the substrate, respectively;
- BP07 and BP08, with a 2 × 2 stoichiometric (001) brucite-like slab (initial s.g. $P\bar{3}m1$), placing the phospholipid with the –PO_4 group pointing outwards and towards the substrate, respectively;
- BP09 and BP10, with a 3 × 2 Al-bearing (001) brucite-like slab (initial s.g. $P\bar{3}m1$), placing the phospholipid with the –PO_4 group pointing outwards and towards the substrate, respectively;
- BP11 and BP12, with a 2 × 2 Al-bearing (001) brucite-like slab (initial s.g. $P\bar{3}m1$), placing the phospholipid with the –PO_4 group pointing outwards and towards the substrate, respectively.

In models BP05, BP06, BP09 and BP10, the surface coverage was 2.0 molecules nm^{-2} (here referred as intermediate coverage), whereas models BP07, BP08, BP11 and BP12 presented 2.8 molecules nm^{-2} (high coverage). PDOS and COOP analyses for models BP05–08 (stoichiometric B layer) and BP09–12 (Al-bearing B substrate) were reported in Figs.S4 and S5, respectively, in the Supplemental Materials.

Results for the intermediate coverage models were graphically shown in Fig. 5, whereas energy features associated with the adsorption process were reported in Table 3. It is worth noting that, for these systems, the preferred way to assess if the molecule is adsorbed onto the mineral substrate is by considering the BSSE-corrected binding energy value net of the lateral interaction term (BE_L^C).

The general results depicted by the simulations can be summarised as follows. First, the phosphatidic acid clearly showed very high lateral interactions between its replicas in neighbouring cells, with ΔE_L values ranging between −76.11 kJ mol^{-1} and − 131.69 kJ mol^{-1}. This figure is mostly given by the dispersive interactions between the valeric acid chains, as suggested by the pure electronic ΔE_L values. Interestingly, in the systems with intermediate phospholipid coverage (BP05, BP06, BP09, and BP10) the lateral interaction was still negative when the long-range interaction contribution was removed; when the surface coverage increased to 2.8 molecules nm^{-2}, the electronic ΔE_L became positive.

Secondly, the DVPA molecule preferred to interact with the (001) brucite-like surface with the phosphate head rather than with the fatty acid tails, as indicated by the differences in the binding energy between models with the same surface slab. The difference between the BE_L^C values calculated for the models with the PO_4 group pointing towards the stoichiometric slab (BP06, BP08) and the corresponding ones where the phosphate head was oriented upwards (BP05, BP07) was about −60 kJ mol^{-1}, a value that increased to ca. –210 kJ mol^{-1} with Al^{3+}/Mg^{2+} substitutions on the (001) mineral surface. This can be explained from the PDOS/COOP data, which showed a high hybridization of the O states of the B layer with those of the molecular groups of the phospholipid in the BP06, BP08, BP10 and BP12 models, whereas the orbitals of the molecule and substrates are less overlapped in energy in the BP05, BP07, BP09 and BP11 systems (see **Figs.S4** and **S5**).

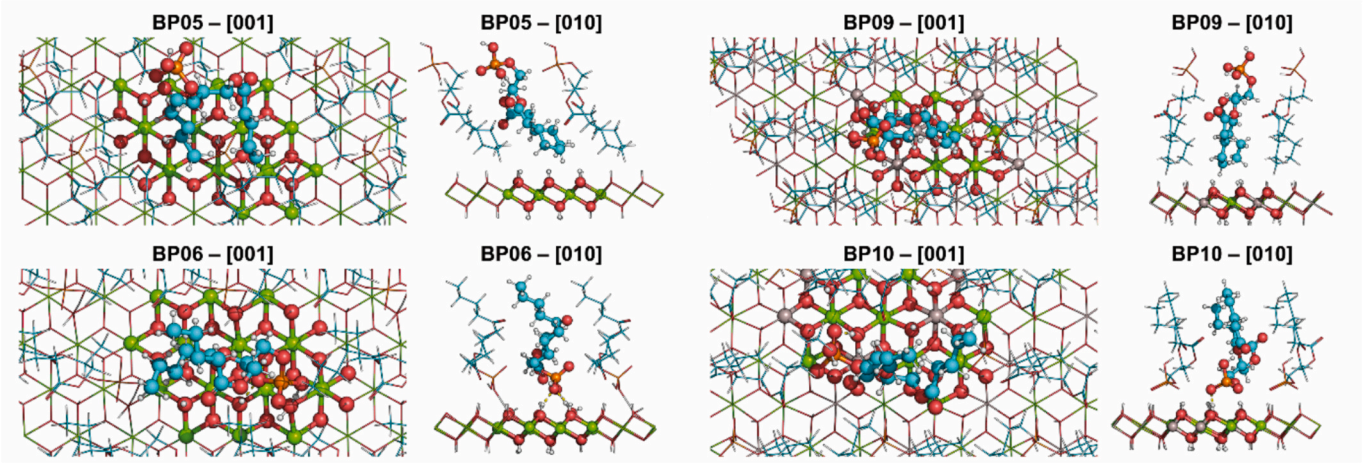

Fig. 5. Views along the [001] and [010] directions of the optimized BP05, BP06, BP09 and BP10 models. Hydrogen bonds (polar contacts) between the phospholipid and the (001) mineral surface are shown in yellow dashed lines. For the sake of clarity, the atoms belonging to the 2D cell used for the simulations were displayed as ball-and-stick models, conversely, the two-dimensional replicas were drawn as wireframes. Colour coding for atoms: P – orange, Al – grey, Mg – green, O – red, C – cyan, H – white. (For interpretation of the references to colour in this figure legend, the reader is referred to the web version of this article.)

Table 3
Binding energies *BE* (uncorrected for the basis set superposition error, BSSE), *BE** (binding energy without contributions from substrate deformation energy δE_S, molecular deformation ΔE_M, and lateral molecular interactions ΔE_L), BE^{*C}, BE^C (*BE* and *BE** corrected for BSSE) and BE_L^C (BE^C net from ΔE_L) associated with the high-coverage adsorption of DVPA onto the brucite-like layer of clinochlore. The energy values are in kJ mol^{-1}.

System	*BE*	*BE**	δE_S	δE_M	ΔE_M	ΔE_L	BE^{*C}	BE^C	*BSSE*	BE_L^C
	Electronic + DFT-D3 energy									
BP05	−169.22	−65.55	2.88	−106.55	14.23	−120.78	−51.95	−155.62	13.60	−34.85
BP06	−233.60	−477.54	83.44	160.50	275.91	−115.41	−458.07	−214.13	19.48	−98.72
BP07	−34.90	−184.59	20.91	128.79	204.90	−76.11	−174.38	−24.68	10.22	51.43
BP08	−110.87	−453.36	106.35	236.15	316.48	−80.34	−432.67	−90.18	20.69	−9.84
BP09	−144.29	−73.76	2.75	−73.27	21.79	−95.06	−61.15	−131.68	12.61	−36.62
BP10	−447.09	−857.85	93.30	317.46	449.15	−131.69	−829.50	−418.74	28.35	−287.05
BP11	−20.16	−51.93	57.26	−25.49	71.92	−97.41	−40.04	−8.27	11.89	89.14
BP12	−222.38	−682.74	92.65	367.71	447.19	−79.48	−658.97	−198.61	23.77	−119.13
	Electronic energy									
BP05	−1.23	8.10	4.66	−13.99	12.02	−26.01	21.70	12.37	13.60	38.38
BP06	−43.00	−391.46	87.47	260.99	281.51	−20.52	−371.98	−23.52	19.48	−3.01
BP07	144.72	−130.59	6.84	268.48	218.02	50.46	−120.37	154.94	10.22	104.49
BP08	89.74	−378.25	92.30	375.69	331.59	44.10	−357.56	110.43	20.69	66.32
BP09	26.66	22.21	6.16	−1.70	20.35	−22.05	34.82	39.27	12.61	61.32
BP10	−240.33	−757.16	97.86	418.97	449.66	−30.69	−728.80	−211.98	28.35	−181.29
BP11	168.53	2.86	42.70	122.96	85.43	37.53	14.75	180.42	11.89	142.89
BP12	−8.33	−605.29	78.15	518.81	462.58	56.23	−581.52	15.44	23.77	−40.78

The third general observation regards the surface coverage, where the models presenting 2.0 molecules nm^{-2} showed more negative binding energy compared to those with larger coverage (2.8 molecules nm^{-2}). For the systems BP07 (stoichiometric substrate) and BP11 (Al-defective brucite-like slab), the adsorption was not stable as the BE_L^C values were largely positive even by including the contribution from long-range interactions. This result suggested that a surface coverage greater than 2.0 is not preferred, especially when the interaction involved the fatty acid chains of the DVPA molecule.

No polar contacts between the phosphatidic acid and the stoichiometric (001) B surface were established in models BP05 and BP07. However, when DVPA was oriented with the phosphate head towards the mineral slab, several hydrogen bonds were formed between the oxygen atoms of the PO_4 group (P = O and P – O – H), with mean length ~ 1.87–1.96 Å, and one of the hydrogen atoms of the polar head was transferred to the surface, forming a trapped water molecule on the slab as observed in the BP03 model (low coverage). In general, the C – C, C – H, C – O and P – O bond lengths did not vary significantly (differences <1.0 %), with the exception of the C = O and C – O – C ones in the BP07 system, which were about 4 % greater than those measured in the gas-phase DVPA. This is due to the long-range polar contacts (~2.3 Å) between the replicas of the molecule between neighbouring cells involving the carbonyl oxygen atoms of the fatty acid chains, which resulted in longer C – O bonds because of the depletion of the electrons cloud of O. As a further consequence, the energy of deformation of the molecule in the BP07 model (ΔE_M = +205 kJ mol^{-1}) was about one order of magnitude greater than the corresponding one in the BP05 adsorption system (intermediate coverage, ΔE_M = +14 kJ mol^{-1}). In the BP06 and BP08 models, the high deformation energy of the phospholipid (+276 kJ mol^{-1} and + 317 kJ mol^{-1}, respectively) was instead mainly ascribable to the proton transfer between the molecule and the substrate. Furthermore, while in the models with 2.0 molecule nm^{-2} the variation of the C_a–C_a–C_a–C_a (intra-chain) and C_a–C_a–O–C_g dihedral angles were in line with those observed in the single-molecule systems (BP01–03), the higher coverage in models BP07 and BP08 caused severe variations in the C_a–C_a–C_a–C_a angular values up to about 13 % in absolute terms. This is due to the reduced distance between the phosphatidic acid molecules imposed by the smaller surface area of the mineral slab, which required more structural variations to accommodate DVPA in the adsorbate/adsorbent system.

Interestingly, in the BP09 system (DVPA on defective brucite-like layer), a single polar contact was established between the terminal –CH_3 group of the second fatty acid chain of the phosphatidic acid and the oxygen near the Al-substituted site, with length 1.94 Å. A similar behaviour was observed in the high-coverage case (model BP11), however the interaction distance was greater (~2.30 Å). When DVPA was oriented with the polar group towards the substrate (models BP10 and BP12), (i) one of the hydrogen atom of the –PO_4H_2 head was transferred to the oxygen atom of the (001) brucite-like surface and (ii) three hydrogen bonds were formed between the molecule and the mineral, with lengths in the range 1.58–2.07 Å. These results explained on one side the high molecular deformation energy of these systems (about +450 kJ mol^{-1}), and on the other side the strong adsorption (very negative binding energy) between the phospholipid and the mineral surface, which is maintained even when the energy contribution from long-range interactions is neglected (see the pure electronic energy in Table 3). Beside the proton transfer, the high ΔE_M values were also due to a combination of variations in the C – O bond lengths, especially for the BP10 model, and in the C_a–C_a–C_a–C_a and C_a–C_a–O–C_g (4.7 %) dihedral angles, whose maximum absolute difference were about 13 % and 4.7 %, respectively.

3.5. Increased coverage of phospholipid on the talc-like layer

As performed for the brucite-like layer, an increase in phospholipid coverage onto the TOT layer was simulated using smaller (001) talc-like surfaces. In this case, the starting 1 × 1 geometries of both stoichiometric and Al-bearing substrates were suitable for a surface coverage of 2.0 molecules nm^{-2}. Considering the results obtained for the BP07, BP08 and BP12 adsorption systems, higher surface coverages were not considered.

Two models, TP03 and TP04, were created placing the phospholipid vertically with respect to the stoichiometric talc-like slab, with the phosphate group orientated outwards and towards the surface, respectively. Then, models TP05 and TP06 were realised with the same molecular orientations of the phosphatidic acid, using the Al-bearing TOT layer as adsorption substrate. The results of the geometry optimization procedure on the TP03–06 models were graphically shown in Fig. 6, and the details of the different contributions to the binding energy were reported in Table 4.

In general, the adsorption of DVPA resulted in the molecule being stably bound to the mineral surface, with BE_L^C values of about −40 kJ mol^{-1} for the stoichiometric TOT layer (TP03 and TP04), whereas a stronger adsorption was observed for the TP05 (BE_L^C ~ −70 kJ mol^{-1}) and TP06 models (BE_L^C ~ −90 kJ mol^{-1}). Differently from the B layer, the process was entirely driven by van der Waals interactions, even when the zeolitic-type Brønsted-Lowry site was involved. Indeed, the electronic binding energy is highly positive for the TP03–05 models, and

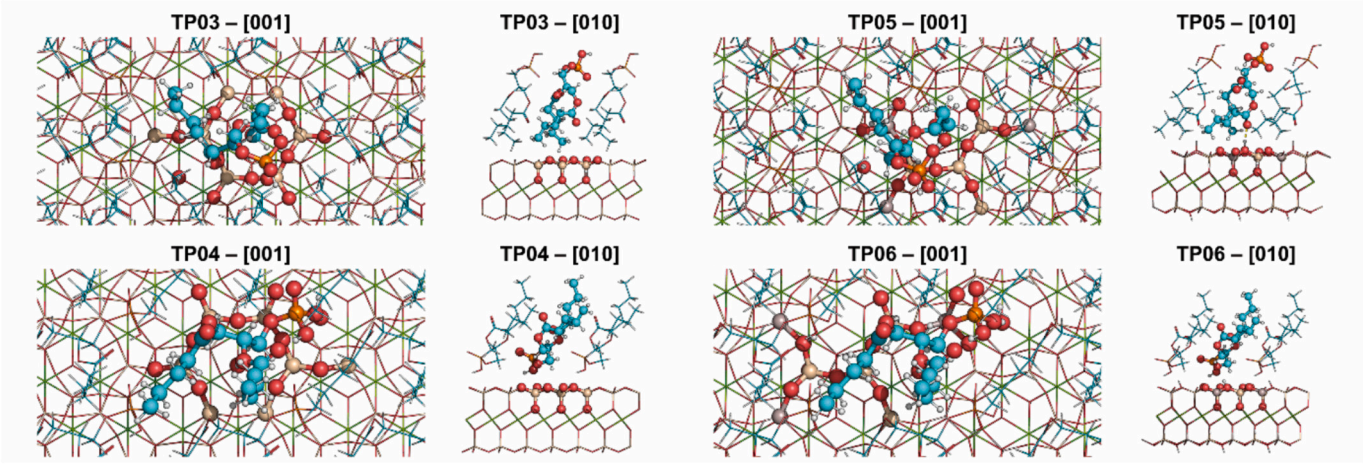

Fig. 6. Views along the [001] and [010] directions of the optimized TP03, TP04, TP05 and TP06 models. Hydrogen bonds (polar contacts) between the phospholipid and the (001) mineral surface are shown in yellow dashed lines. For clarity, the atoms belonging to the 2D cell used for the simulations were displayed as ball-and-stick models, conversely, the two-dimensional replicas were drawn as wireframes. Colour coding for atoms: P – orange, Si – dark yellow, Al – grey, Mg – green, O – red, C – cyan, H – white. (For interpretation of the references to colour in this figure legend, the reader is referred to the web version of this article.)

Table 4
Binding energies *BE* (uncorrected for the basis set superposition error, BSSE), *BE** (binding energy without contributions from substrate deformation energy δE_S, molecular deformation ΔE_M, and lateral molecular interactions ΔE_L), BE^{*C}, BE^C (*BE* and *BE** corrected for BSSE) and BE_L^C (BE^C net from ΔE_L) associated with the high-coverage adsorption of DVPA onto the TOT layer of clinochlore. The energy values are in kJ mol^{-1}.

System	*BE*	*BE**	δE_S	δE_M	ΔE_M	ΔE_L	BE^{*C}	BE^C	*BSSE*	BE_L^C
	Electronic + DFT-D3 energy									
TP03	−165.89	−69.60	2.28	−98.58	16.52	−115.11	−59.98	−156.28	9.62	−41.17
TP04	−192.25	−84.76	3.57	−111.06	25.32	−136.38	−71.53	−179.03	13.23	−42.65
TP05	−195.68	−120.76	7.98	−82.90	26.55	−109.45	−107.49	−182.41	13.27	−72.96
TP06	−245.48	−153.77	12.51	−104.22	31.44	−135.66	−137.13	−228.84	16.64	−93.17
	Electronic energy									
TP03	18.31	28.43	−0.47	−9.64	16.29	−25.93	38.04	27.93	9.62	53.86
TP04	14.67	6.61	1.96	6.10	17.48	−11.38	19.83	27.90	13.23	39.28
TP05	6.95	−14.78	2.70	19.04	24.66	−5.63	−1.51	20.22	13.27	25.85
TP06	−31.51	−56.57	16.97	8.09	22.33	−14.24	−39.92	−14.86	16.64	−0.62

a very small and negative value was calculated for the TP06 one. The slab deformation energy δE_S was very small and in the 2.3–12.5 kJ mol^{-1} range, meaning that the phosphatidic acid only slightly affected the geometry of the substrate.

When the DVPA molecule was oriented with the phosphate group outwards the surface (stoichiometric TP03 and Al-defective TP05 models), the fatty acid chains did not form any long-range bond with the basal oxygen atoms of the substrate. A single polar bond was found in the TP05 system, which was established between the carbonyl oxygen (C = O) of the second valeroyl chain and the H atom near the Al-substituted site at about 1.83 Å. This was accompanied by a variation of the C_a–C_a–C_a–C_a torsional angle of the same chain of ~13 % with respect to the value calculated for the isolated phospholipid molecule, together with a 5–6 % change in the C_a–C_a–O–C_g dihedral angles of both chains. These variations explained the slightly higher ΔE_M value of the TP04 model (+25 kJ mol^{-1}) compared to that of the TP03 system (+17 kJ mol^{-1}). No significant variations (<1 %) in the C – C, C – H, C – O and P – O bond lengths were observed. Also, more antibonding states were present in the TP03 and TP05 models than in the TP04 and TP06 one (see **Fig.S6**), suggesting a general weakening of the molecular and substrate bonds due to their interaction.

In the TP04 system, where the phosphate group was oriented towards the substrate, a single polar contact was established between one of the OH group of the phosphate head of DVPA and the basal oxygen atoms of the TOT layer, at about 2.00 Å. A similar behaviour was noted in the relaxed TP06 model (1.98 Å), and an additional hydrogen bond at about 1.60 Å was formed between the hydrogen atom of the Brønsted-Lowry site and the oxygen atom of the OH group of the phosphate head that was involved in the other polar contact (see Fig. 6). In both TP04 and TP06 models, the variations of the C_a–C_a–C_a–C_a and C_a–C_a–O–C_g torsional angles were similar (mean absolute values of ~3 % and ~ 5 %, respectively), and the bond lengths were almost constant with respect to the isolated phospholipid. Compared to the TP03 and TP05 models, the formation of the polar contacts required a small variation in the orientation of the OH groups of the phosphate head, which was reflected in the slightly higher deformation energy of the molecule in the TP04 and TP06 systems.

4. Discussion and conclusions

In the present work, a detailed atomic-scale analysis of the interaction of a model phospholipid, i.e., the 1, 2-divaleroyl-*sn*-glycero-3-phosphatidic acid (DVPA) with the brucite-like (B) and talc-like (TOT) layers was performed with DFT simulations, aiming at a deeper understanding of the adsorption of membrane lipids with clinochlore and, in general, with clay minerals. For a fruitful discussion, the adsorption results on the different substrates were compared initially for the single-molecule case, followed by those related to the ideal formation of a DVPA monolayer. In the former situation, the adsorption of the biomolecule onto the stoichiometric B and TOT layer (models BP01–02 and TP01) was very similar from the energy perspective, with an absolute binding energy in the range 130–140 kJ mol^{-1}, which is due to the long-range interactions of both the valeric acid chains and the polar head with the substrate. The BP03 system showed a slightly different

behaviour compared to the BP01 and BP02, showing a proton transfer from the $–PO_4H_2$ head to the brucite-like surface during the optimization procedure, hence polar (Coulombic) interactions between the negatively charged molecule and the positive surface were established, increasing the binding energy. This peculiar and specific result in the BP03 system was instead the main observable in the BP04 model, where the Brønsted-Lowry basic site on the B layer due to the Al^{III}/Mg^{II} substitution (Moro et al., 2019b) led to a very strong negative electrostatic surface potential (ESP) that favourably interacted with the positive electrostatic molecular potential (EMP) on the $–PO_4H_2$ head, leading to the same proton transfer and an almost double binding energy value ($BE^C = -371$ kJ mol^{-1}). The acidic BL site on the TOT layer (model TP02) provided a much lower increase in binding energy (about 30 kJ mol^{-1} from the value of TP01) compared to the basic BL site in the BP04 system, which was ascribed to less favourable interactions between the positive ESP and positive EMP. In fact, the polar contact between the phosphatidic head and the surface involved the hydrogen atom of the Brønsted-Lowry site (Al – O – H) and the oxygen atom of one of the acidic OH groups of the phospholipid. These observations at single molecule level were in line with previous observations related to the adsorption of both simple (Valdrè et al., 2011; Moro et al., 2020) and complex biomolecules, such as nucleotides (Valdrè, 2005), RNA/DNA (Valdrè et al., 2011), amino acids (Moro et al., 2015, 2019b, 2020) and proteins (Pignataro et al., 2020) on the brucite-like and talc-like layers.

The formation of a lipid monolayer was simulated using (001) slab models of the two clinochlore layers with reduced surface areas and placing DVPA normal to the substrate. Differently from the single-molecule case, the results generally showed a clear adsorption preference for the amphiphilic molecule onto the (001) brucite-like surface when DVPA was oriented with the polar head pointing towards the slab. Furthermore, the binding energy BE^L_C of the Al-substituted B layer (model BP10) was three times that of the stoichiometric substrate (model BP06) and Al-substituted BP10), highlighting the strong electrostatic interaction between the polar phosphate head and the basic Brønsted-Lowry site. However, when DVPA interacted with the terminal $–CH_3$ groups of the fatty acid tails with the BL site of the brucite-like surface, the BE^L_C value was not significantly affected, suggesting a weak coupling between the electrostatic potentials of the molecule and the substrate. Regarding the stoichiometric talc-like layer, the calculated binding energy values were similar irrespective of the phospholipid orientation (~ -41 kJ mol^{-1}), resulting in a less specific, i.e., selective adsorption of DVPA onto this substrate. These BE^L_C increased in absolute terms by about 30–50 kJ mol^{-1} when the acidic Brønsted-Lowry site (Al^{III}/Si^{IV} substitution) was present on the TOT slab, which was ascribed to the polar interaction, i.e., hydrogen bond formation between the Al–O–H of the talc-like surface and the C═O carbonyl group (valeric acid chain) in model TP05, and the OH group (phosphatidic head) in model TP06.

Considering the hydrophobic/hydrophilic nature of the brucite-like and talc-like layers, respectively, and the presence of water or other polar solvents in supported lipid bilayer technology, when phospholipids are deposited onto a cleaved clinochlore substrate from a solution there could be a subtle interplay between the two (001) surfaces during the condensation and self-assembly processes. Indeed, it was shown that SLBs formed on silica substrates generally maintain a $\sim$ 1 nm thick H_2O layer between the membrane and the solid surface, which preserves most of the properties of free membranes (Gromelski et al., 2009). Albeit in the absence of water, the hypothesis suggested by the simulations of the present work is that this water layer between the phospholipids and the substrate could be present when the adsorption occurs on the TOT layer; conversely, this solvent layer could be thinner or even absent onto the hydrophobic B layer, with more direct interaction between the lipids and the mineral surface. Dehydration and re-hydration processes, typically occurring in prebiotic chemistry environments, could also modify the self-assembly of the phospholipid bilayers onto clinochlore, with dehydration driving more molecules towards the B layer. Work is in progress to verify this hypothesis using AFM-based techniques in liquid and atmospheric environments, which would pave new roads in the comprehension of the events that led to the formation of the membranes in simple proto-cells. Also, AFM could be used to experimentally verify and validate the conformation of the molecules here predicted for low and high surface coverage of DVPA.

The present study also showed that too high surface coverage led to a certain degree of instability in the phospholipid layer on the surface relative to lower-coverage systems. Generally, the equilibrium distance between the molecules was measured at 8 Å per phosphate head in a phospholipid bilayer (membrane) in a water medium (Zimmerberg, 2006). This distance was about 7.8 Å in the phospholipid/brucite-like slab models with a surface coverage of about 2.0 molecules nm^{-2}, which reduced to $\sim$6.5 Å when the coverage increased to 2.8 molecules nm^{-2}. When the adsorption involved the TOT layer, the distance between the phosphate heads in neighbouring cells was about 7.2 Å. The high DVPA coverage in the BP07, BP08, BP11 and BP12 systems brought the molecules too close to each other, with a high steric hindrance that increased the repulsion between the fatty acid chains and required large variations in the phospholipid conformation to minimize these interactions, eventually resulting in a less favourable adsorption process. In the other considered models with 2.0 molecules nm^{-2}, the distance between the phospholipids was in line with the one reported by Zimmerberg (2006), considering that the simulations were carried out in athermal conditions (0 K) and the absence of solvent (H_2O).

Compared to previous studies, the results presented in this work were in line with the neutron reflectivity and quartz crystal microbalance measurements of the formation of 1, 2-dimyristoyl phosphatidilcholine (DMPC) lipid bilayer on bare and functionalized (with a polyelectrolyte multilayer, PEM) silica SiO_2 surface (Gromelski et al., 2009). The PEM was also functionalized with either poly(sodium 4-styrenesulfonate) or poly(allylamine hydrochloride) to obtain a negative or positive charge, respectively, on the multilayer surface. In the cited work, it was shown that a homogeneous DMPC bilayer was preferentially formed on the negatively charged surface than on the positively charged one, with the polar head oriented towards the functionalized PEM. Notwithstanding the very different substrate employed by Gromelski and collaborators (2009), the simulation of the adsorption of DVPA on the Al-substituted brucite-like layer, which presented a negative surface potential, confirmed the experimental observations. Furthermore, considering the hydrophobic behaviour and the low binding energy towards water (Moro et al., 2019b), the (001) brucite-like surface could be a suitable atomic-flat surface to stably adsorb phospholipids for biological/biochemical applications were polar solvents are employed.

The present findings were in line with the experimental observations of Wicklein et al. (2016), who investigated the intercalation phosphatidylcoline (PC) in sepiolite and 2:1 Mg/Al LDH. In the former case, the phospholipid was intercalated within the modulated layers of the mineral, with PC forming a polar bond with the siloxane oxygen via the polar head. Intercalation was not observed when using the LDH substrate, instead, the phospholipid was adsorbed onto the mineral surface. The adsorption mechanism suggested by infrared spectroscopy involved the formation of hydrogen bonds between the phospholipid (from the $–PO_4$ polar head and the carbonyl C = O groups) and the substrate. The present simulations involving the Al-bearing brucite-like layer, which resembles the building block of the 2:1 Mg/Al LDH, confirmed the hypothesis of Wicklein and collaborators (2016). Although sepiolite is different from the talc-like layer because of the modulation of the TOT layers, the results obtained from the stoichiometric TP04 model showed polar bonds between the $–PO_4$ group of DVPA and the siloxane rings, which agrees with the formation of the lipid monolayer observed by Wicklein et al. (2016).

In the grand canonical Monte Carlo simulations at molecular mechanics level proposed by Pertsin and Grunze (2014), the authors investigated the behaviour of a 1,2-dilauroyl-phosphatidyl-

ethanolamine (DLPE) monolayer on mica, with a hydration layer between the biomolecules and the mineral substrate. Four models were realised considering different distances h between the monolayer and the muscovite surface where the separations were associated with normal pressures acting on the phospholipids. When $h = 28$ Å, it was noted the formation of a N – H — O hydrogen bonds between the terminal $–NH_3^+$ group of one of the DLPE molecules and an oxygen atom of the tetrahedral sheet of the mica substrate. In addition, strong electrostatic interactions were established between the phosphate group of the biomolecule and the nearest potassium cations of muscovite. According to these observations, the authors proposed an adsorption mechanism where some individual lipid molecules protrude from the bilayer, passing through the water layer between the SLB and the substrate, to form stable bonds with the mineral surface. The simulation protocol of Pertsin and Grunze (2014) did not allow the estimation of the free energy of adhesion for the simulated membrane onto the (001) muscovite surface. Nevertheless, although no water molecules were considered in the present DFT simulations, the results here provided for DVPA onto clinochlore confirmed the formation of strong polar bonds between the polar group and the negatively charged surface of the brucite-like layer.

The authors are aware that the considered phospholipid molecule, i.e., DVPA is a very simple model for the building blocks of both cell membranes and supported lipid bilayers. In addition, the effects associated with water molecules that are typically present in both biological and pharmaceutical/technological systems were neglected in the present simulations. However, the present study is a suitable basic and necessary starting point for providing a deeper understanding of the intimate relationship between clinochlore and phospholipids. DVPA presented all the physical and chemical characteristics of these biomolecules, i.e., the hydrophilic polar head and the hydrophobic fatty acid tails, which provided the required different adsorption behaviour expected from more complex phospholipids, e.g., phosphatidylcholines. Performing high-accuracy simulations within the Density Functional Theory framework for very complex systems, i.e., with larger mineral substrates, increased number of long phospholipids and several (hundreds of) water molecules is still a tremendous task from the computational perspective. Machine-learning approaches, for instance, moment tensor potentials (Shapeev, 2016) that are trained on DFT results and (mostly) provide the same accuracy could be used as a suitable alternative. Moreover, the role of other minor and trace elements (e.g., Fe, Ti, Cr) present in the clinochlore structure on the adsorption behaviour of phospholipids needs to be carefully assessed. Work is in progress by the authors of the present paper to consider these effects.

A deeper knowledge of the interactions between clay minerals and phospholipids is of utmost importance for the employment of the formers for environmental and (bio)technological applications. The present theoretical study related to the adsorption of a simple model of phospholipid (DVPA) onto clinochlore, a mineral with interesting and peculiar properties for the adsorption, condensation and (self-)organisation of different hydrophobic/hydrophilic biomolecules, could be very helpful for devising innovative biotechnological applications of this substrate in a lab-on-a-chip (or lab-on-a-mineral) devices (Xu et al., 2010) or proposing new derived substrates.

CRediT authorship contribution statement

Gianfranco Ulian: Writing – review & editing, Visualization, Validation, Methodology, Investigation, Formal analysis, Data curation, Conceptualization. **Giacomo Trondoli:** Writing – review & editing, Methodology, Investigation, Formal analysis, Data curation. **Francesca Ranellucci:** Writing – review & editing, Visualization, Methodology, Investigation, Formal analysis. **Giovanni Valdrè:** Writing – review & editing, Validation, Supervision, Investigation, Formal analysis, Conceptualization.

Declaration of competing interest

The authors declare that they have no known competing financial interests or personal relationships that could have appeared to influence the work reported in this paper.

Data availability

Input and output files produced with the CRYSTAL code are deposited in a dedicated dataset, freely available at https://doi.org/10.17632/5vrdhj5h7f.1.

Acknowledgements

The authors wish to thank the University of Bologna for supporting the present research. All the simulations were performed with the computational resources (HPC cluster) and software license of the Interdisciplinary Research Centre of Biomineralogy, Crystallography and Biomaterials, Department of Biological, Geological and Environmental Sciences, University of Bologna.

Appendix A. Supplementary data

Supplementary data to this article can be found online at https://doi.org/10.1016/j.clay.2025.108053.

References

Cell mediated calcification and matrix vesicles: proceedings of the 4. Internat. Conference on Matrix Vesicles, Cambridge, 1–5 July 1985, Excerpta medica International congress series. In: Ali, S.Y. (Ed.), 1986. Presented at the International Conference on Matrix Vesicles, Excerpta Medica, Amsterdam.

Antognozzi, M., Wotherspoon, A., Hayes, J.M., Miles, M.J., Szczelkun, M.D., Valdrè, G., 2006. A chlorite mineral surface actively drives the deposition of DNA molecules in stretched conformations. Nanotechnology 17, 3897–3902. https://doi.org/10.1088/0957-4484/17/15/047.

Bagatolli, L.A., Stock, R.P., 2021. Lipids, membranes, colloids and cells: a long view. Biochim. Biophys. Acta Biomembr. 1863. https://doi.org/10.1016/j.bbamem.2021.183684.

Becke, A.D., 1993a. Density-functional thermochemistry. 3. the role of exact exchange. J. Chem. Phys. 98, 5648–5652. https://doi.org/10.1063/1.464913.

Becke, A.D., 1993b. A New Mixing of Hartree-Fock and Local Density-Functional Theories. J. Chem. Phys. 98, 1372–1377. https://doi.org/10.1063/1.464304.

Boskey, A.L., 2007. Mineralization of bones and teeth. Elements 3, 385–391. https://doi.org/10.2113/gselements.3.6.385.

Boys, S.F., Bernardi, F., 1970. The calculation of small molecular interactions by the differences of separate total energies. Some procedures with reduced errors. Mol. Phys. 19, 553–566.

Brezesinski, G., Möhwald, H., 2005. Polyelectrolyte coupling with lipid monolayers. Mol. Interfacial Phenomena Polym. Biopolymers. 286–322. https://doi.org/10.1533/9781845690830.2.286.

Broyden, C.G., 1970a. The convergence of a class of double-rank minimization algorithms: 1. General considerations. IMA J. Appl. Math. 6, 76–90. https://doi.org/10.1093/imamat/6.1.76.

Broyden, C.G., 1970b. The convergence of a class of double-rank minimization algorithms: 2. The new algorithm. IMA J. Appl. Math. 6, 222–231. https://doi.org/10.1093/imamat/6.3.222.

Catti, M., Pavese, A., Aprà, E., Roetti, C., 1993. Quantum-mechanical Hartree-Fock study of calcite (CaCO3) at variable pressure, and comparison with magnesite ($MgCO_3$). Phys. Chem. Miner. 20, 104–110. https://doi.org/10.1007/BF00207203.

De La Pierre, M., Orlando, R., Maschio, L., Doll, K., Ugliengo, P., Dovesi, R., 2011. Performance of six Functionals (LDA, PBE, PBESOL, B3LYP, PBE0, and WC1LYP) in the simulation of Vibrational and Dielectric Properties of Crystalline Compounds. The Case of Forsterite Mg2SiO4. J. Comput. Chem. 32, 1775–1784. https://doi.org/10.1002/jcc.21750.

Erba, A., Desmarais, J.K., Casassa, S., Civalleri, B., Donà, L., Bush, I.J., Searle, B., Maschio, L., Edith-Daga, L., Cossard, A., Ribaldone, C., Ascrizzi, E., Marana, N.L., Flament, J.P., Kirtman, B., 2023. CRYSTAL23: a program for Computational Solid State Physics and Chemistry. J. Chem. Theory Comput. 19, 6891–6932. https://doi.org/10.1021/acs.jctc.2c00958.

Fletcher, R., 1970. A new approach to variable metric algorithms. Comput. J. 13, 317–322. https://doi.org/10.1093/comjnl/13.3.317.

Fuerstenau, D.W., Pradip, 2005. Zeta potentials in the flotation of oxide and silicate minerals. Adv. Colloid Interf. Sci. 114–115, 9–26. https://doi.org/10.1016/j.cis.2004.08.006.

Gatti, C., Saunders, V.R., Roetti, C., 1994. Crystal-field effects on the topological properties of the electron-density in molecular-crystals - the case of urea. J. Chem. Phys. 101, 10686–10696. https://doi.org/10.1063/1.467882.
Goldfarb, D., 1970. A family of variable-metric methods derived by variational means. Math. Comput. 24, 23–26. https://doi.org/10.1090/S0025-5718-1970-0258249-6.
Grimme, S., Antony, J., Ehrlich, S., Krieg, H., 2010. A consistent and accurate ab initio parametrization of density functional dispersion correction (DFT-D) for the 94 elements H-Pu. J. Chem. Phys. 132, 154104. https://doi.org/10.1063/1.3382344.
Grimme, S., Ehrlich, S., Goerigk, L., 2011. Effect of the Damping Function in Dispersion Corrected Density Functional Theory. J. Comput. Chem. 32, 1456–1465. https://doi.org/10.1002/jcc.21759.
Grimme, S., Brandenburg, J.G., Bannwarth, C., Hansen, A., 2015. Consistent structures and interactions by density functional theory with small atomic orbital basis sets. J. Chem. Phys. 143. https://doi.org/10.1063/1.4927476.
Gromelski, S., Saraiva, A.M., Krastev, R., Brezesinski, G., 2009. The formation of lipid bilayers on surfaces. Colloids Surf. B: Biointerfaces 74, 477–483. https://doi.org/10.1016/j.colsurfb.2009.08.006.
Hancock, J.F., 2006. Lipid rafts: Contentious only from simplistic standpoints. Nat. Rev. Mol. Cell Biol. 7, 456–462. https://doi.org/10.1038/nrm1925.
Heinz, H., 2012. Clay minerals for nanocomposites and biotechnology: surface modification, dynamics and responses to stimuli. Clay Miner. 47, 205–230. https://doi.org/10.1180/claymin.2012.047.2.05.
Jurak, M., 2014. Surface Gibbs energy interaction of phospholipid/cholesterol monolayers deposited on mica with probe liquids. Chem. Phys. Lipids 183, 60–67. https://doi.org/10.1016/j.chemphyslip.2014.05.007.
Lambert, J.F., 2008. Adsorption and polymerization of amino acids on mineral surfaces: a review. Orig. Life Evol. Biosph. 38, 211–242. https://doi.org/10.1007/s11084-008-9128-3.
Lee, C.T., Yang, W.T., Parr, R.G., 1988. Development of the Colle-Salvetti Correlation-Energy Formula into a Functional of the Electron-Density. Phys. Rev. B 37, 785–789. https://doi.org/10.1103/PhysRevB.37.785.
Lingwood, D., Simons, K., 2010. Lipid Rafts as a Membrane-Organizing Principle. Science 327, 46–50. https://doi.org/10.1126/science.1174621.
McConnell, H.M., Watts, T.H., Weis, R.M., Brian, A.A., 1986. Supported planar membranes in studies of cell-cell recognition in the immune system. BBA - Rev. Biomembr. 864, 95–106. https://doi.org/10.1016/0304-4157(86)90016-X.
Monkhorst, H.J., Pack, J.D., 1976. Special points for Brillouin-zone integrations. Phys. Rev. B 8, 5188–5192.
Moro, D., Ulian, G., Valdrè, G., 2015. Single molecule investigation of glycine–chlorite interaction by cross-correlated scanning probe microscopy and quantum mechanics simulations. Langmuir 31, 4453–4463. https://doi.org/10.1021/acs.langmuir.5b00161.
Moro, D., Ulian, G., Valdrè, G., 2016. Nanoscale cross-correlated AFM, Kelvin probe, elastic modulus and quantum mechanics investigation of clay mineral surfaces: the case of chlorite. Appl. Clay Sci. 131, 175–181. https://doi.org/10.1016/j.clay.2015.11.023.
Moro, D., Ulian, G., Valdrè, G., 2019a. 3D meso-nanostructures in cleaved and nanolithographed Mg-Al-hydroxysilicate (clinochlore): Topology, crystal-chemistry, and surface properties. Appl. Clay Sci. 169, 74–80. https://doi.org/10.1016/j.clay.2018.12.020.
Moro, D., Ulian, G., Valdrè, G., 2019b. Amino acids-clay interaction at the nano-atomic scale: the l-alanine-chlorite system. Appl. Clay Sci. 172, 28–39. https://doi.org/10.1016/j.clay.2019.02.013.
Moro, D., Ulian, G., Valdrè, G., 2020. Nano-atomic scale hydrophobic/philic confinement of peptides on mineral surfaces by cross-correlated SPM and quantum mechanical DFT analysis. J. Microsc. 280, 204–221. https://doi.org/10.1111/jmi.12923.
Nada, R., Nicholas, J.B., McCarthy, M.I., Hess, A.C., 1996. Basis sets for ab initio periodic Hartree-Fock studies of zeolite/adsorbate interactions: he, Ne, and Ar in silica sodalite. Int. J. Quantum Chem. 60, 809–820. https://doi.org/10.1002/(SICI)1097-461X(1996)60:4<809::AID-QUA3>3.0.CO;2-0.
Pascale, F., Zicovich-Wilson, C.M., Orlando, R., Roetti, C., Ugliengo, P., Dovesi, R., 2005. Vibration frequencies of $Mg_3Al_2Si_3O_{12}$ pyrope. An ab initio study with the CRYSTAL code. J. Phys. Chem. B 109, 6146–6152. https://doi.org/10.1021/jp050316z.
Perdikatsis, B., Burzlaff, H., 1981. Structural refinement of talc $Mg_3Si_4O_{10}(OH)_2$. Z. Krist. 156, 177–186. https://doi.org/10.1524/zkri.1981.156.3-4.177.
Pertsin, A., Grunze, M., 2014. Possible mechanism of adhesion in a mica supported phospholipid bilayer. J. Chem. Phys. 140. https://doi.org/10.1063/1.4875020.
Pietrement, O., Castro-Smirnov, F.A., Le Cam, E., Aranda, P., Ruiz-Hitzky, E., Lopez, B.S., 2018. Sepiolite as a New Nanocarrier for DNA transfer into Mammalian Cells: Proof of Concept, issues and Perspectives. Chem. Rec. 18, 849–857. https://doi.org/10.1002/tcr.201700078.
Pignataro, M., Di Rocco, G., Lancellotti, L., Bernini, F., Subramanian, K., Castellini, E., Bortolotti, C.A., Malferrari, D., Moro, D., Valdrè, G., Borsari, M., Monte, F.D., 2020. Phosphorylated cofilin-2 is more prone to oxidative modifications on Cys39 and favors amyloid fibril formation. Redox Biol. 37. https://doi.org/10.1016/j.redox.2020.101691.
Prencipe, M., Scanavino, I., Nestola, F., Merlini, M., Civalleri, B., Bruno, M., Dovesi, R., 2011. High-pressure thermo-elastic properties of beryl ($Al_4Be_6Si_{12}O_{36}$) from ab initio calculations, and observations about the source of thermal expansion. Phys. Chem. Miner. 38, 223–239. https://doi.org/10.1007/s00269-010-0398-8.
Reimhult, E., Höök, F., Kasemo, B., 2003. Intact vesicle adsorption and supported biomembrane formation from vesicles in solution: Influence of surface chemistry, vesicle size, temperature, and osmotic pressure. Langmuir 19, 1681–1691. https://doi.org/10.1021/la0263920.
Shanno, D.F., 1970. Conditioning of quasi-Newton methods for function minimization. Math. Comput. 24, 647–656. https://doi.org/10.1090/S0025-5718-1970-0274029-X.
Shapeev, A.V., 2016. Moment Tensor Potentials: a Class of Systematically Improvable Interatomic Potentials. Multiscale Model. Simul. 14, 1153–1173. https://doi.org/10.1137/15M1054183.
Stueckenschneider, K., Merz, J., Schembecker, G., 2014. Molecular Interaction of Amino Acids with Acidic Zeolite BEA: the effect of Water. J. Phys. Chem. C 118, 5810–5819. https://doi.org/10.1021/jp411734j.
Ulian, G., Valdrè, G., 2015. Density functional investigation of the thermo-physical and thermo-chemical properties of 2M1 muscovite. Am. Mineral. 100, 935–944. https://doi.org/10.2138/am-2015-5086.
Ulian, G., Valdrè, G., 2019. Equation of state and second-order elastic constants of portlandite ca$(OH)_2$ and brucite $Mg(OH)_2$. Phys. Chem. Miner. 46, 101–117. https://doi.org/10.1007/s00269-018-0989-3.
Ulian, G., Valdrè, G., 2023. Crystal-chemical, vibrational and electronic properties of 1M-phlogopite $K(Mg,Fe)_3Si_3AlO_{10}(OH)_2$ from Density Functional Theory simulations. Appl. Clay Sci. 246, 107166. https://doi.org/10.1016/j.clay.2023.107166.
Ulian, G., Moro, D., Valdrè, G., 2018. First principle investigation of the mechanical properties of natural layered nanocomposite: Clinochlore as a model system for heterodesmic structures. Compos. Struct. 202, 551–558. https://doi.org/10.1016/j.compstruct.2018.02.089.
Ulian, G., Moro, D., Valdrè, G., 2020. Infrared and Raman spectroscopic features of clinochlore $Mg_6Si_4O_{10}(OH)_8$: a density functional theory contribution. Appl. Clay Sci. 197, 105779. https://doi.org/10.1016/j.clay.2020.105779.
Ulian, G., Moro, D., Valdrè, G., 2021a. DFT simulation of the Water Molecule Interaction with the (00l) Surface of Montmorillonite. Minerals 11, 501. https://doi.org/10.3390/min11050501.
Ulian, G., Moro, D., Valdrè, G., 2021b. Water adsorption behaviour on (001) pyrophyllite surface from ab initio Density Functional Theory simulations. Appl. Clay Sci. 212, 106221. https://doi.org/10.1016/j.clay.2021.106221.
Ulman, A., 1996. Formation and Structure of Self-Assembled Monolayers. Chem. Rev. 96, 1533–1554. https://doi.org/10.1021/cr9502357.
Valdrè, G., 2005. Atomic force microscopy observation of agglomerates, ordered structures and filaments after deposition of DNA nucleotides onto layer silicate mineral surfaces. Scanning 27, 100–101.
Valdrè, G., 2007. Natural nanoscale surface potential of clinochlore and its ability to align nucleotides and drive DNA conformational change. Eur. J. Mineral. 19, 309–319. https://doi.org/10.1127/0935-1221/2007/0019-1732.
Valdrè, G., Fabrizioli, S., 2006. The role of layer silicate substrates on immobilization of red blood cells. SCANNING 28, 72–73.
Valdrè, G., Malferrari, D., Brigatti, M.F., 2009. Crystallographic Features and Cleavage Nanomorphology of Chlinochlore: specific applications. Clay Clay Miner. 57, 183–193. https://doi.org/10.1346/Ccmn.2009.0570205.
Valdrè, G., Moro, D., Ulian, G., 2011. Nucleotides, RNA and DNA selective adsorption on atomic-flat Mg–Al-hydroxysilicate substrates. Micro Nano Lett. 6, 922–926. https://doi.org/10.1049/mnl.2011.0546.
Valdrè, Giovanni, Moro, D., Ulian, G., 2011a. Interaction of organic molecules with layer silicates, oxides and hydroxides and related surface-nano-characterization techniques. In: Brigatti, M.F., Mottana, A. (Eds.), Layered Mineral Structures and Their Application in Advanced Technologies, European Mineralogical Union Notes in Mineralogy, pp. 313–334.
Valdrè, Giovanni, Tosoni, S., Moro, D., 2011b. Zeolitic-type 'Bronsted-Lowry sites distribution imaged on clinochlore. Am. Mineral. 96, 1461–1466. https://doi.org/10.2138/am.2011.3774.
Valenzano, L., Torres, F.J., Doll, K., Pascale, F., Zicovich-Wilson, C.M., Dovesi, R., 2006. Ab initio study of the vibrational spectrum and related properties of crystalline compounds; the case of $CaCO_3$ calcite. Zeitschrift Fur Physikalische Chemie-International Journal of Research in Physical Chemistry & Chemical Physics 220, 893–912. https://doi.org/10.1524/zpch.2006.220.7.893.
Valenzano, L., Noel, Y., Orlando, R., Zicovich-Wilson, C.M., Ferrero, M., Dovesi, R., 2007. Ab initio vibrational spectra and dielectric properties of carbonates: magnesite, calcite and dolomite. Theor. Chem. Accounts 117, 991–1000. https://doi.org/10.1007/s00214-006-0213-2.
Wicklein, B., Darder, M., Aranda, P., Del Burgo, M.A.M., Del Real, G., Esteban, M., Ruiz-Hitzky, E., 2016. Clay-lipid nanohybrids: Towards influenza vaccines and beyond. Presented at the. Clay Miner. 529–538. https://doi.org/10.1180/claymin.2016.051.4.01.
Xu, J., Stevens, M.J., Oleson, T.A., Last, J.A., Sahai, N., 2009. Role of Oxide Surface Chemistry and Phospholipid phase on Adsorption and Self-Assembly: Isotherms and Atomic Force Microscopy. J. Phys. Chem. C 113, 2187–2196. https://doi.org/10.1021/jp807680d.
Xu, Y., Takai, M., Ishihara, K., 2010. Phospholipid Polymer Biointerfaces for Lab-on-a-Chip Devices. Ann. Biomed. Eng. 38, 1938–1953. https://doi.org/10.1007/s10439-010-0025-3.
Zhang, X.V., Kendall, T.A., Hao, J., Strongin, D.R., Schoonen, M.A.A., Martin, S.T., 2006. Physical Structures of Lipid Layers on Pyrite. Environ. Sci. Technol. 40, 1511–1515. https://doi.org/10.1021/es051794q.
Zicovich-Wilson, C.M., Bert, A., Roetti, C., Dovesi, R., Saunders, V.R., 2002. Characterization of the electronic structure of crystalline compounds through their localized Wannier functions. J. Chem. Phys. 116, 1120–1127. https://doi.org/10.1063/1.1425406.
Zimmerberg, J., 2006. Membrane biophysics. Curr. Biol. 16, R272–R276. https://doi.org/10.1016/j.cub.2006.03.050.